Journal of Power Sources 196 (2011) 116–125

Contents lists available at ScienceDirect

Journal of Power Sources

journal homepage: www.elsevier.com/locate/jpowsour

Effect of PH_3 poisoning on a Ni-YSZ anode-supported solid oxide fuel cell under various operating conditions

Chunchuan Xu [a,*], John W. Zondlo [a], Mingyang Gong [b], XingBo Liu [b]

[a] Department of Chemical Engineering, West Virginia University, Morgantown, WV 26506, USA
[b] Department of Mechanical & Aerospace Engineering, West Virginia University, Morgantown, WV 26506, USA

ARTICLE INFO

Article history:
Received 11 June 2010
Received in revised form 6 July 2010
Accepted 7 July 2010
Available online 13 July 2010

Keywords:
SOFC
Ni-YSZ anode
Coal syngas
Phosphine contaminant
Nickel phosphide

ABSTRACT

The Ni-YSZ anode-supported solid oxide fuel cell (SOFC) can generate electrical power by using coal-derived syngas as the fuel. However, trace contamination of phosphine (PH_3) in the syngas can cause irreversible degradation in cell performance. A series of tests at 10 ppm PH_3 in the fuel gas was carried out under a variety of operating conditions, viz, with/without electrochemical reaction in syngas and with/without H_2O in H_2 fuel at 750 °C, 800 °C and 850 °C. The poisoning effects were evaluated by both electrochemical methods and chemical analyses. The post-mortem analyses of the SOFC anode were performed by means of XRD, SEM/EDS, and XPS. The results show that the degradation rate is larger at the higher cell working temperature using syngas with PH_3 in a 200 h test though PH_3 is more reactive with Ni in the anode at lower working temperature and produces a secondary nickel phosphide (Ni_xP_y) phase. The dominant compositions of Ni_xP_y on the cell anode are Ni_5P_2 with the presence of H_2O, and $Ni_{12}P_5$ without the presence of H_2O. The production of Ni_xP_y can be generated on the cell anode using syngas or dry H_2 fuel with 10 ppm PH_3 contaminant. Further, the appearance of Ni_xP_y phases is independent of the electrochemical reactions in the cell.

1. Introduction

The poisoning effect on the Ni-YSZ anode-supported cell using snygas fuel has been investigated at 800 °C in previous papers [1,2]. This paper will explore the poisoning effect for variations of the SOFC working temperature and fuel compositions. Several researchers have reported the effects of PH_3 in syngas mixtures and H_2 fuel on Ni-YSZ anodes, and nickel phosphide (Ni_xP_y) compounds were identified as products on the Ni-YSZ anode surface [3,4]. But it is unclear whether or not the formation of Ni_xP_y is related to SOFC working temperature, electrochemical reactions or H_2O present in the reactions.

In this paper, we report extended tests on commercial SOFC button cells with Ni-YSZ composite anodes in a syngas mixture and dry H_2 both containing 10 ppm PH_3. The current collector is arranged to expose the central part of the anode to the fuel gas mixture without any intervening metal grid or metal paste. Periodic evaluation of impedance assesses the ohmic and polarization resistances during the experiment. Extensive post-mortem analyses by SEM, XRD and XPS are used to evaluate the chemical and microstructural changes in the anode. These results are compared to the previous reports and to thermodynamic predictions.

2. Experimental methods

2.1. SOFC and test setup

In this study, commercial anode-supported solid oxide button cells and Ni-YSZ cermet discs manufactured by Materials and Systems Research Inc. (MSRI) were used. The detailed description of the cell composition, structure, dimensions and cell contact configuration has been reported in a previous paper [1]. Mass flow controllers were employed to control the flow rates of H_2, CO, CO_2, N_2/PH_3 (1000 ppm PH_3 in a balance of nitrogen) and air separately. A temperature-controlled humidifier was used to adjust the H_2O concentration of the simulated coal syngas fed to the anode. The total syngas (30% H_2, 26% H_2O, 23% CO and 21% CO_2) and dry H_2 fuel flow rate was kept constant at approximately 200 standard cubic centimeters per minute (sccm) and the air-flow rate was held at approximately 300 sccm. For syngas fuel, the anode fuel transfer lines were heat-traced to over 120 °C so that water condensation between the humidifier and furnace was prevented. CO, CO_2 and PH_3 were injected downstream of the anode humidifier close to the furnace into a ceramic (Al_2O_3) inlet tube to ensure that all trace species in the stream reached the anode of the SOFC

* Corresponding author at: Department of Chemical Engineering, West Virginia University, Morgantown, WV 26506-6012, USA. Tel.: +1 304 293 9379; fax: +1 304 293 4139.
E-mail address: Chunchuan.Xu@mail.wvu.edu (C. Xu).

0378-7753/$ – see front matter © 2010 Elsevier B.V. All rights reserved.
doi:10.1016/j.jpowsour.2010.07.018

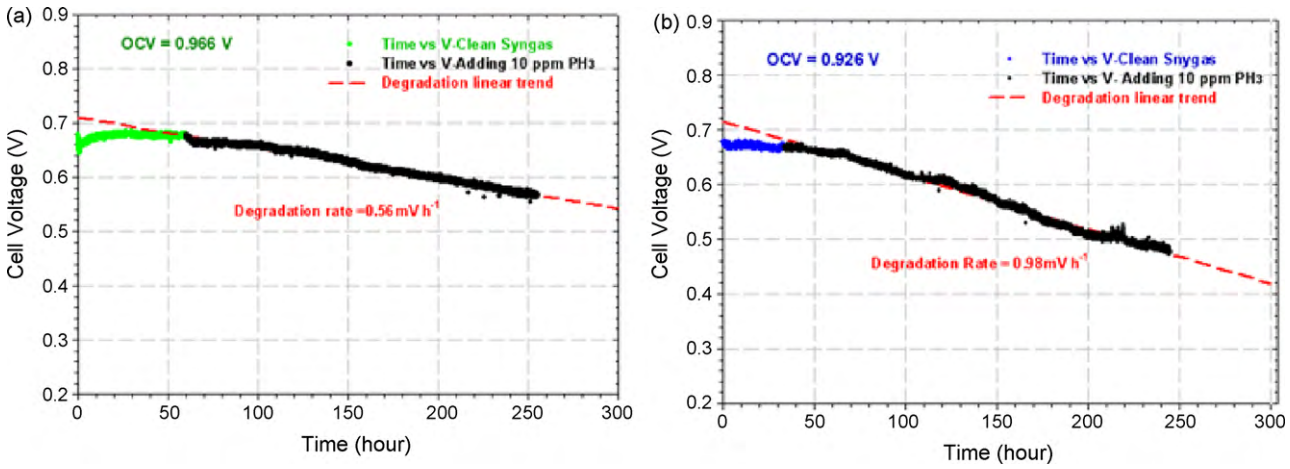

Fig. 1. The cell voltage versus time under 0.5 A cm^{-2} load operating on syngas before and after adding 10 ppm PH_3 at (a) 750 °C and (b) 850 °C.

in a minimum amount of time. For the test with dry H_2 fuel, the H_2 by-passed the humidifier, was mixed with PH_3 close to the furnace and then delivered to the cell anode or Ni-YSZ cermet disc.

2.2. Electrochemical testing of the SOFC

The cell tests followed the same procedure which was described in the previous paper [1]. To investigate the temperature-related effects for the PH_3 poisoning, the cells were further tested with syngas fuel at 750 °C and 850 °C. The cell OCVs were recorded and showed reasonable agreement with the theoretical values at specific temperatures. The cell OCV, voltage under 0.5 A cm^{-2} load and degradation rates for all the tests have been recorded. Impedance spectra were taken periodically during cell testing after adding PH_3. The impedance spectra were collected using a Solartron SI 1260 impedance/gain-phase analyzer with AC amplitude of 20 mV at frequencies ranging from 100 kHz to 0.1 Hz. To inspect whether or not the PH_3-poisoning effects on Ni-YSZ anode were related to the electrochemical reactions, a Ni-YSZ cermet disc (without electrolyte and cathode) was tested at 850 °C by loading syngas with 10 ppm PH_3 on one side of the Ni-YSZ cermet disc while the other side was sealed by a mica membrane which prevented air from reaching this surface. After each cell test was completed, the anode side was purged with 80% N_2 and 20% H_2 while being cooled to room temperature in about 4 h. This purge minimized the exposure of the cell anode to ambient air. To investigate the correlation between PH_3-poisoning effects and H_2O present on the cell anode, one cell was run under 0.5 A cm^{-2} load, and a second cell was kept at OCV when using dry H_2 fuel for about 120 h at 800 °C. The cell impedances were taken periodically during the testing.

2.3. Morphology, chemical and thermodynamic analyses

The microstructure and chemical composition of the cell anode were examined with a Hitachi S-4700 SEM/EDS. To determine the composition of the anode, an XRD (Panalytical X'Pert Pro PM-3040) with a Cu K-alpha radiation source (1.54060 Å), and an XPS (PHI 5000 VerasProbe XPS Microprobe) with a monochromatic Al K-alpha radiation source (8.34118 Å) were employed. Thermodynamic analysis was carried out with the FACTSAGE 5.4 software package.

3. Experimental results

3.1. The poisoning effect of PH_3 in syngas at 750 °C and 850 °C

After accounting for a slight change in cell performance during the initial break-in period (loading at a constant current density of 0.5 A cm^{-2}), the cell voltage under load was stable over 24 h in coal syngas. Following the introduction of 10 ppm PH_3, the cell performance quickly starts to degrade (Fig. 1). Both cells were run for about 200 h after adding 10 ppm PH_3. The average cell degradation rates under 0.5 A cm^{-2} constant current density are 0.56 mV h^{-1} for the 750 °C case and 0.98 mV h^{-1} for the 850 °C case. The performance loss is nearly double at the cell working temperature of 850 °C than that at 750 °C. These two "as-received" MSRI cells were made in the same batch which means the cells have the same

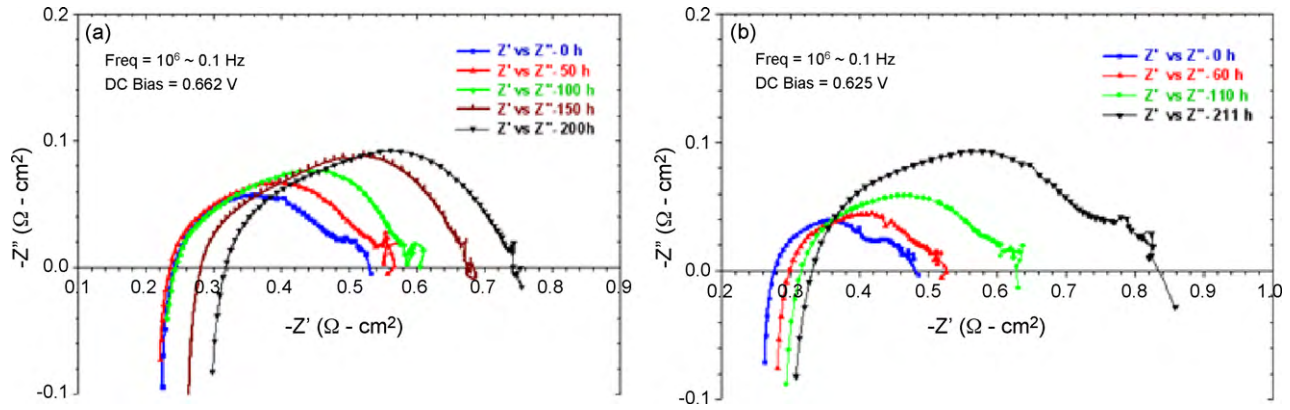

Fig. 2. The normalized impedance spectra of the cells in syngas before and during exposure to 10 ppm PH_3 at (a) 750 °C and (b) 850 °C.

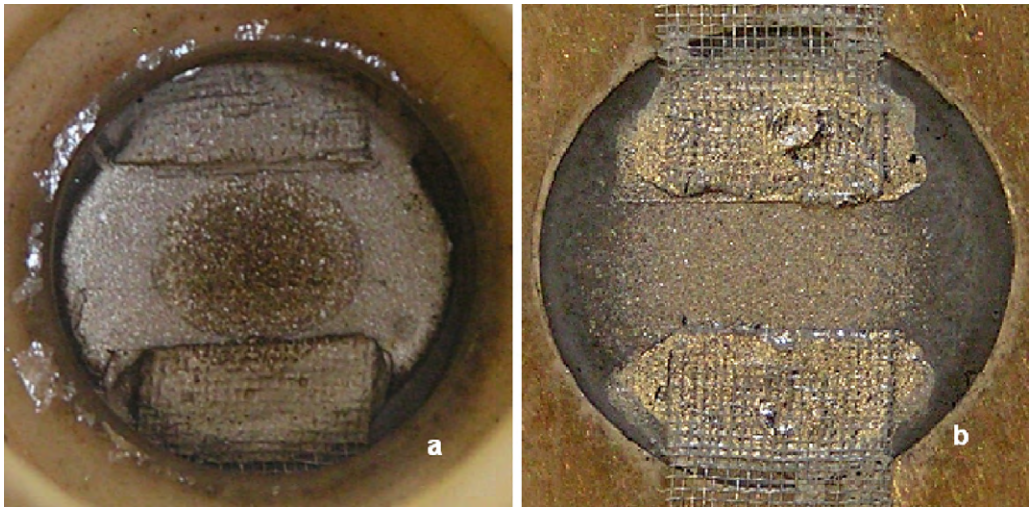

Fig. 3. Post-mortem PH_3-poisoned cell anodes (2 cm diameter) at (a) 750 °C and (b) 850 °C. The visible anode area diameter is 2 cm.

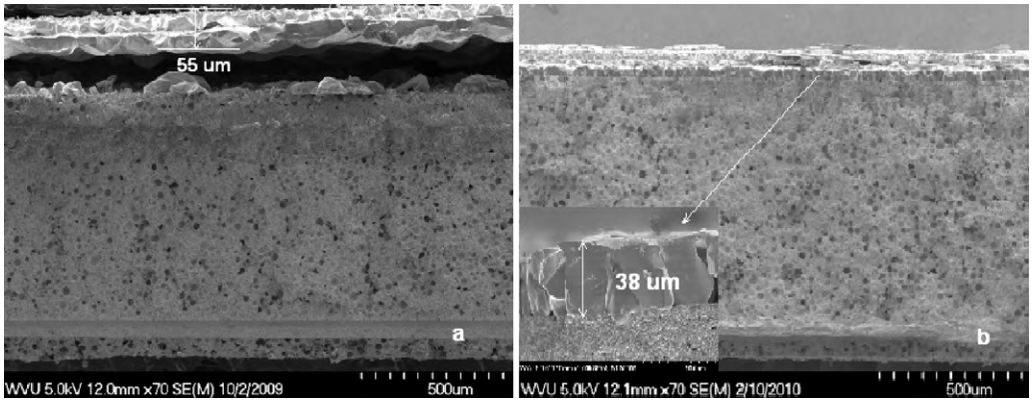

Fig. 4. The SEM micrographs of the entire anode cross-section after exposure to syngas with 10 ppm PH_3 for about 200 h at (a) 750 °C and (b) 850 °C.

structure and composition. However the cell performance may vary slightly for different cells and cell testing conditions. After finishing the test, the cell was cooled to room temperature by purging with 20% H_2 and 80% N_2 to prevent oxidation of the cell anode.

The impedance spectra under a DC bias show that the ohmic resistance (high frequency intercept with Z' axis) and the total polarization resistance (low frequency intercept with Z' axis) both increase with increasing time of exposure to PH_3 (Fig. 2). Before adding PH_3, the cell ohmic resistance R_Ω and total cell resistance R_{total} (area specific resistance) are about 0.24 Ω cm^2 and 0.53 Ω cm^2 for 750 °C case and 0.28 Ω cm^2 and 0.48 Ω cm^2 for 850 °C case respectively. After adding PH_3 for about 200 h, the observed increase of the ohmic resistance ΔR_Ω and the total cell resistance ΔR_{total} is listed in Table 1 for both cases. The ΔR_{total} is significantly larger for the higher temperature case than for the lower temperature case.

Post-mortem photographs of the PH_3-poisoned cell anode are shown in Fig. 3(a) and (b). Both poisoned anode surfaces show a shiny metallic material covering the open surface area of the anode and significant loss of the anode pore structure. In these surface pictures, the pattern formations of Ni_xP_y are slightly different in the two cases. The center-cell surface layer at 850 °C (Fig. 3(b)) showed

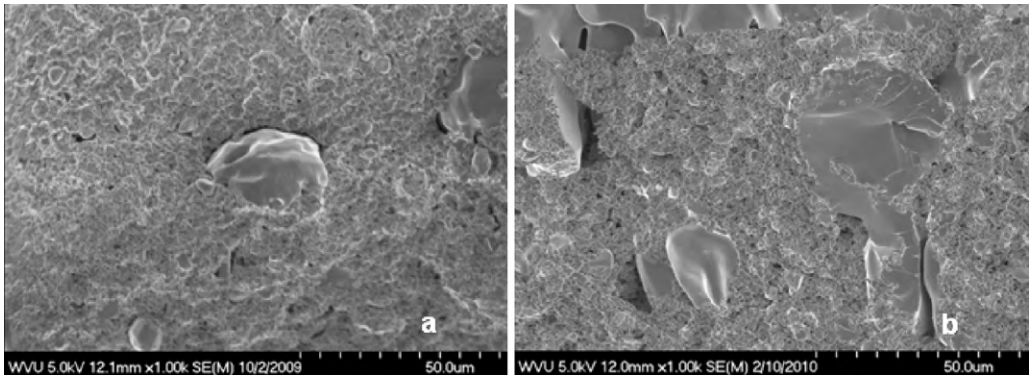

Fig. 5. SEM images near the top 50 μm of the cell anode cross-section after exposure to syngas with 10 ppm PH_3 for about 200 h at (a) 750 °C and (b) 850 °C.

Table 1
Summary of test results from the PH_3-poisoning experiments.

Cell working condition	OCV[a] experimental	Load ($A\,cm^{-2}$) for time	Cell resistance ΔR_{Ω} and ΔR_{total}	Voltage loss at load 0.5 $A\,cm^{-2}$	Major Ni_xP_y XRD peak
Syngas at 750 °C	0.966 V	0.5 for 200 h	0.08 and 0.22 $\Omega\,cm^2$	110 mV	Ni_5P_2
Syngas at 850 °C	0.926 V	0.5 for 211 h	0.05 and 0.35 $\Omega\,cm^2$	198 mV	Ni_5P_2
Syngas at 850 °C (Ni-YSZ disc)	–	0.0 for 120 h	–	–	Ni_5P_2
Dry H_2 at 800 °C cell-1	1.102 V	0.5 for 113 h	0.13 and 0.28 $\Omega\,cm^2$	95 mV	Ni_5P_2
Dry H_2 at 800 °C cell-2	1.102 V	0.0 for 140 h	0.04 and 0.28 $\Omega\,cm^2$	65 mV	$Ni_{12}P_5$

[a] The OCV is measured under fuel flow about 200 sccm.

a more metallic shine than that at 750 °C (Fig. 3(a)). The shiny layer coverage area is larger in the 750 °C case than that of the 850 °C case. The cross-sectional image of the 750 °C cell in Fig. 4(a) shows that a 55 μm Ni_xP_y layer was produced after adding PH_3 and it actually separated from the top anode surface. Comparing this behavior with the 850 °C case in Fig. 4(b), the Ni_xP_y layer is about 38 μm and is fused to the cell anode. This observation indicates that the Ni_xP_y was produced intensively on the cell anode top surface at 750 °C. After the Ni_xP_y was built up over a certain thickness, the Ni_xP_y loses its tight bond with the anode skeleton and delaminates from the cell. This observation also explains why the ohmic resistance in the 750 °C case increased much more than that in the 850 °C case. The microstructure of the top anode layer was significantly reconstructed in the both cases. However, the detailed cross-section SEM images of the anodes show that more and larger agglomerates were formed at 850 °C than at 750 °C (Fig. 5). The change of the inner cell anode microstructure is more severe in the 850 °C case. This image implies that the reactions of PH_3 with Ni penetrate faster and deeper in the cell anode at 850 °C than at 750 °C. The EDS spectra of these agglomerates indicate that the major constituents are Ni and P.

The XRD spectra of the cell anode surface for these two cases have similar patterns, and indicate that the dominant as Ni_xP_y phase is Ni_5P_2 (spectrum a and b in Fig. 6) [5]. The main Ni_5P_2 peaks are the same as those in a previous paper where the cell was tested at 800 °C [1]. The Ni peaks are at 44.17° and 51.49° [6]. There are no NiO peaks present at 37.24° and 43.27° because the cell was cooled in a reducing environment. The only P_2O_5 peak is at 40.31° and is very weak [7]. The positions of the YSZ peaks and the other significant peaks are listed in Table 2 [8].

3.2. PH_3 in syngas reaction with a Ni-YSZ cermet disc at 850 °C

A Ni-YSZ cermet disc was loaded in the test fixture but without making any electrical contacts to the surface. The top side of the disc was fed humidified syngas with 10 ppm PH_3 at 850 °C, and the other side was sealed by a mica membrane so that the fuel cannot penetrate through the cell and air is excluded from the cell during the test. Furthermore there are no electrochemical reactions occurring on the Ni-YSZ cermet disc. After 120 h of exposure, the disc was cooled to room temperature by purging N_2 with 20% H_2. The image of the side exposed to syngas with 10 ppm PH_3 is shown in

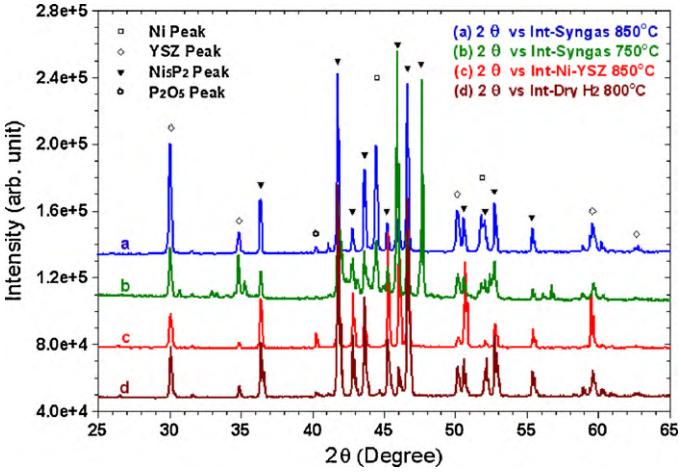

Fig. 6. The XRD spectra of the top cell anode surface after exposure to 10 ppm PH_3 in (a) syngas fuel at 850 °C, (b) syngas fuel at 750 °C, (c) syngas fuel at 850 °C by using Ni-YSZ disc and (d) dry H_2 at 800 °C with 0.5 $A\,cm^{-2}$ load.

Fig. 7(a). There is a small shiny metallic-type bubble about 0.82 cm diameter at the center of the disc. The image of the other side in Fig. 7(b) basically shows the appearance of a uniformly reduced Ni-YSZ cermet, and does not display any notable changes on the surface. The detailed SEM image and the EDS spectrum of the shiny bubble top surface are shown in Fig. 8(a) and (b) respectively. The EDS spectrum confirmed that Ni and P are the major constituents of this material. The cross-sectional image of disc in Fig. 9(a) shows that the convex layer has separated from the Ni-YSZ cermet disc. The layer thickness of the shiny bubble is about 50–70 μm. The detailed image of the Ni-YSZ disc top layer cross-section which is located just under the shiny layer also exhibits the characteristic agglomeration of nickel phosphide (see in Fig. 9(b)).

The XRD spectrum c in Fig. 6 of the shiny bubble area displays the clear and strong Ni_5P_2 series of signals at 2θ positions which are listed in Table 2. The Ni signals are not significantly strong in this spectrum and the YSZ peaks are relative weak compared to those in spectra a and b in Fig. 6 for the previous two cases. The strong Ni_5P_2 peaks imply that the shiny bubble is mostly composed of Ni_5P_2. The single P_2O_5 peak is weak at 40.31°. The metallic shiny bubble is evidence that the 10 ppm PH_3 in syngas is favored to react

Table 2
XRD peak list 2θ°.

YSZ peaks [7]	Ni_5P_2 peaks [4]	Ni peaks [5]	$Ni_{12}P_5$ peaks [8]	P_2O_5 peaks [6]
30.10°	36.40°, 41.78°	44.17°	29.19°, 32.73°	29.55°[a]
34.89°	42.36°, 42.83°	51.49°	35.38°, 35.81°	40.31°
50.21°	43.32°, 45.30°	62.21°[a]	38.41°, 41.25°	46.53°[a]
59.79°	45.95°, 46.62°		41.63°, 46.96°	
62.86°	46.62°, 47.66°		48.96°, 54.04°	
	52.44°, 52.73°		55.85°, 56.15°	
	55.43°, 56.14°		58.02°, 60.14°[a]	
	56.21°			

[a] The peak may be hidden by nearby peaks.

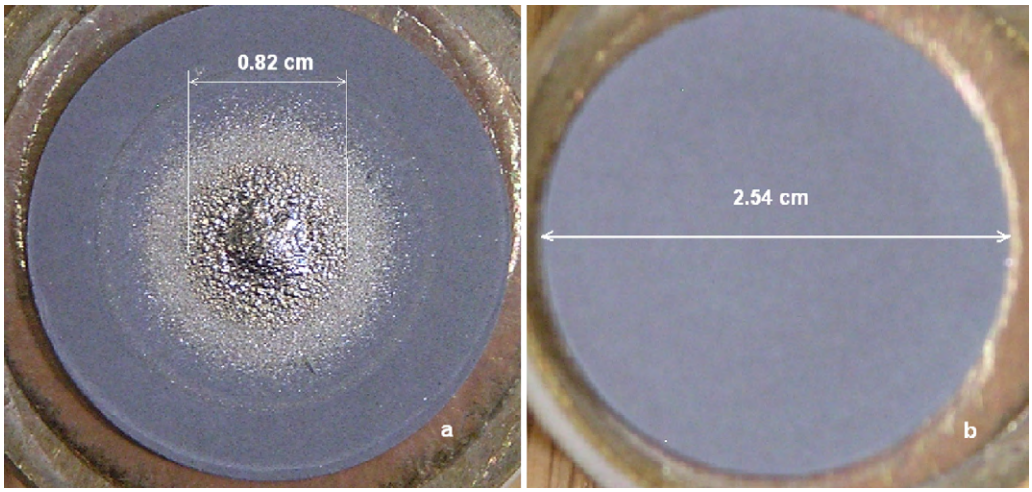

Fig. 7. Ni-YSZ cermet disc exposed to 10 ppm PH_3 in syngas at 850 °C for 120 h. (a) A shiny bubble about 0.82 cm diameter appears on the side facing the syngas with 10 ppm PH_3 and (b) the back side of the disc is a clean reduced Ni-YSZ cermet.

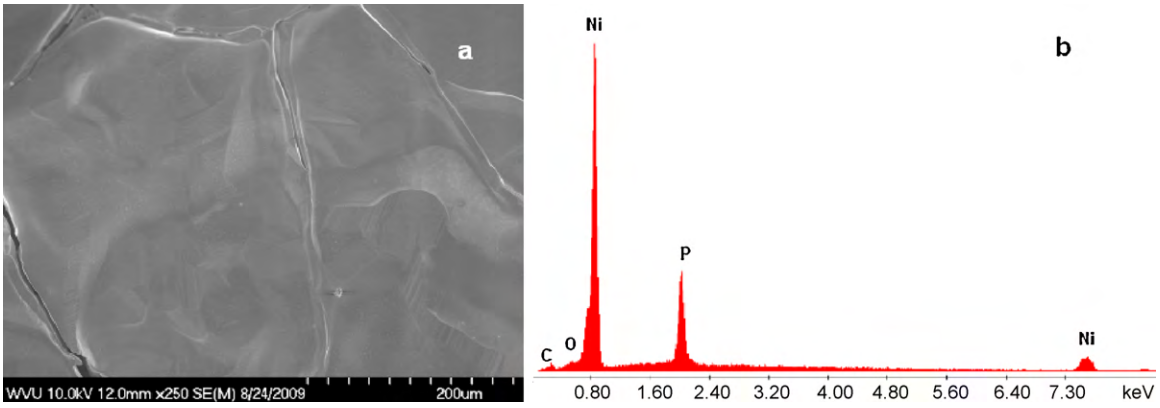

Fig. 8. (a) The detailed SEM image of the shiny bubble top surface and (b) EDS spectrum of the shiny bubble surface displays significant Ni and P signals.

with Ni to produce Ni_xP_y at SOFC typical working temperatures independent of electrochemical reactions.

3.3. *The poisoning effect of PH_3 in dry H_2 fuel at 800 °C*

To investigate whether or not PH_3 poisoning of the Ni-YSZ anode is related to the presence of H_2O vapor in the fuel, the cells were exposed to dry H_2 (ultra high purity hydrogen) with 10 ppm PH_3 as the fuel. Cell-1 was tested under 0.5 A cm^{-2} constant current density for about 120 h of PH_3 exposure. The cell voltage versus the time is shown in Fig. 10(a). The cell degradation rate is about 0.98 mV h^{-1} which is the highest degradation rate for all the cases. The impedance spectra indicate both the ohmic resistance and total cell resistance are increasing with time of the cell exposure to dry H_2 fuel with 10 ppm PH_3 (Fig. 10(b)). Although the H_2O was not intentionally mixed in the H_2 fuel, there is still some H_2O present on the cell anode as a result of the electrochemical reaction under load. A Ni_xP_y layer was produced on the top open anode surface as shown in Fig. 11(a). The top anode cross-sectional SEM micrograph shows a 26 μm thick Ni_xP_y layer on the anode surface in Fig. 12(a).

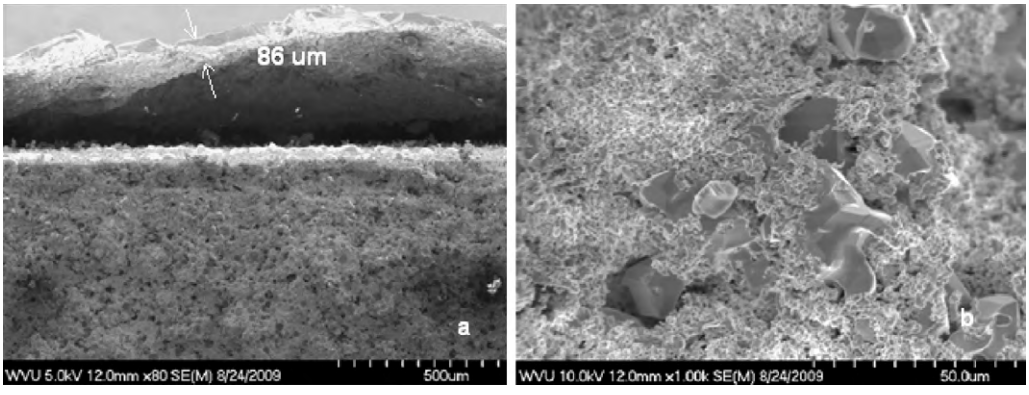

Fig. 9. (a) The cross-sectional image of the Ni-YSZ disc and the shiny bubble above it and (b) the detailed image of the top cross-section of the Ni-YSZ disc.

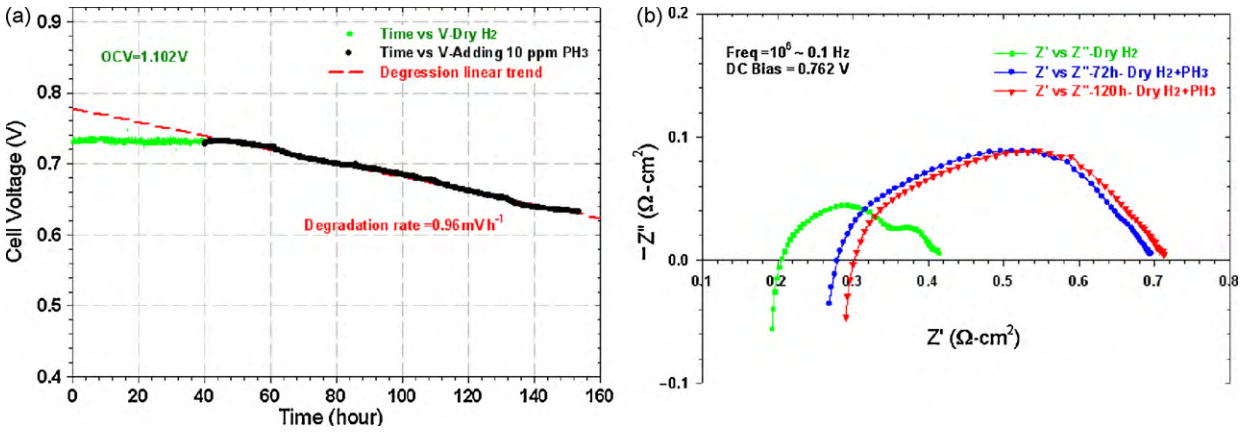

Fig. 10. (a) The cell voltage versus time under load of 0.5 A cm^{-2} and (b) the normalized impedance spectra for a cell operating on dry H_2 before and after adding 10 ppm PH_3 at 800 °C.

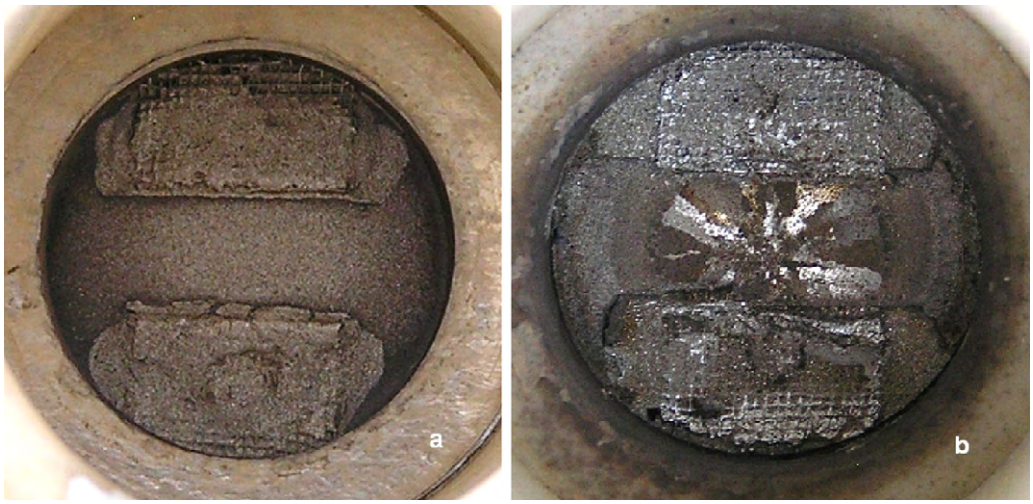

Fig. 11. Post-mortem PH_3-poisoned anode side surface (2 cm diameter) images at (a) dry H_2 fuel with a load of 0.5 A cm^{-2} and (b) dry H_2 fuel without load. The visible anode area diameter is 2 cm.

The XRD spectra of the post-mortem cell anode indicated that the composition of Ni_xP_y is still dominated by Ni_5P_2 (see spectrum d in Fig. 6).

Cell-2 was tested using dry H_2 fuel with 10 ppm PH_3 for 140 h under an open circuit voltage (OCV) condition which avoids completely the presence of H_2O produced by electrochemical reaction on cell anode. The cell OCV was constant at 1.102 V during the test. The impedance data of the cell-2 under DC 640 mV bias were taken at 0 h, 65 h and 140 h and are shown in Fig. 13(a). The increase of the ohmic resistance ΔR_Ω is about 0.04 Ω cm^2 and the increase of the total cell resistance ΔR_{total} is about 0.28 Ω cm^2 after exposure to PH_3 for 140 h. The post-mortem image of cell-2 anode is shown in Fig. 11(b). When compared with cell-1 which was loaded at 0.5 A cm^{-2}, the cell-2 anode surface has been severely reconstructed. A dense shiny layer with an average thickness of about 50–60 μm was built up on the top of open cell anode. The dense

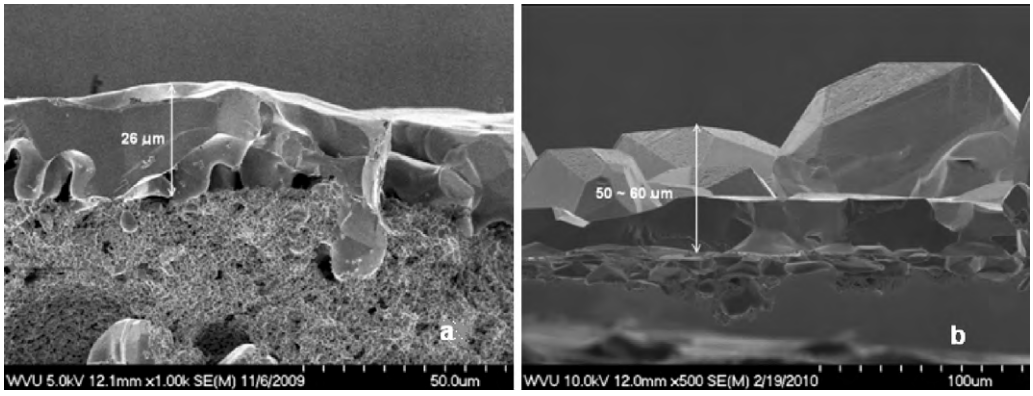

Fig. 12. The SEM micrographs of the top anode cross-section after exposure to dry H_2 with 10 ppm PH_3 at 800 °C. (a) The cell with 0.5 A cm^{-2} load for about 120 h at 1000× magnification and (b) the cell without load for about 140 h at 500× magnification.

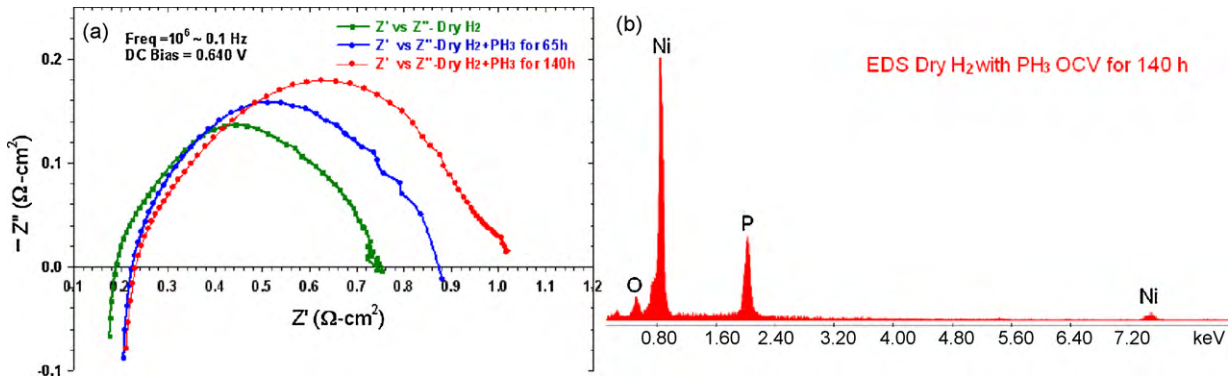

Fig. 13. (a) The normalized impedance spectrum of the cell operating at OCV using dry H_2 with 10 ppm PH_3 at 800 °C and (b) the EDS spectrum of the shiny layer surface at the cross-spot indicated in Fig. 14(b).

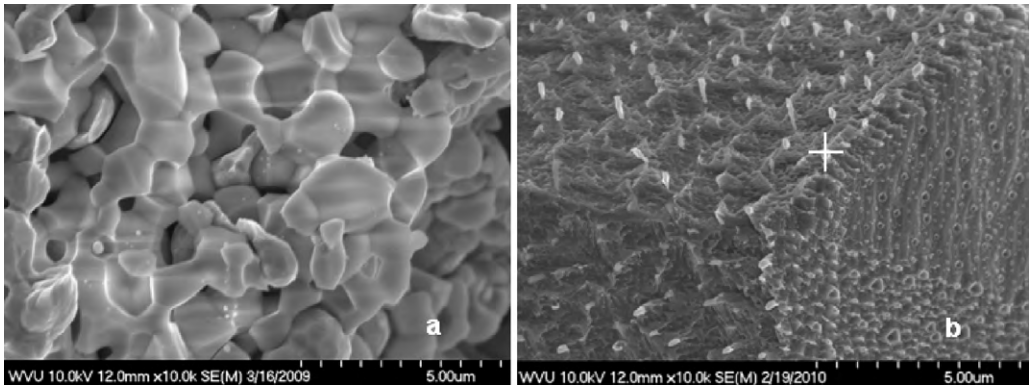

Fig. 14. The detailed SEM micrographs of (a) a clean reduced Ni-YSZ anode surface and (b) the dense layer produced by 10 ppm PH_3 impurity. The EDS spectrum in Fig. 13(b) was taken at the cross-spot of (b).

shiny layer was fractal and mostly detached from the anode (see Fig. 12(b)). The detailed SEM micrographs in Fig. 14(a) and (b) exhibit different microstructures for the clean Ni-YSZ anode surface and the cell-2 dense Ni_xP_y layer on the Ni-YSZ anode after exposure to dry H_2 with 10 ppm PH_3. Under 10 K magnification, the clean Ni-YSZ anode image shows the typical porous structure along with the Ni and YSZ particles. In contrast, the dense shiny layer is uniform and devoid of pores. The chemical analysis carried out by EDS indicated that the chemical constituents of the layer are Ni and P in Fig. 13(b). $Ni_{12}P_5$ was the dominant product identified by the XRD spectrum a in Fig. 15 on the cell anode dense layer [9]. In this spectrum, the major composition of Ni_xP_y is different from spectra b and c for which H_2O was present at the cell anode. The weak P_2O_5 peak was not detected at 40.31°. However, XRD is not sensitive to very low concentration of species.

3.4. Results from XPS examination

XPS was performed on the Ni-YSZ anodes tested in coal syngas at 750 °C, 850 °C and in dry H_2 at 800 °C under OCV (cell-2). The specific elemental electronic states for the surface and the cross-section of the Ni-YSZ anodes were examined at regions located

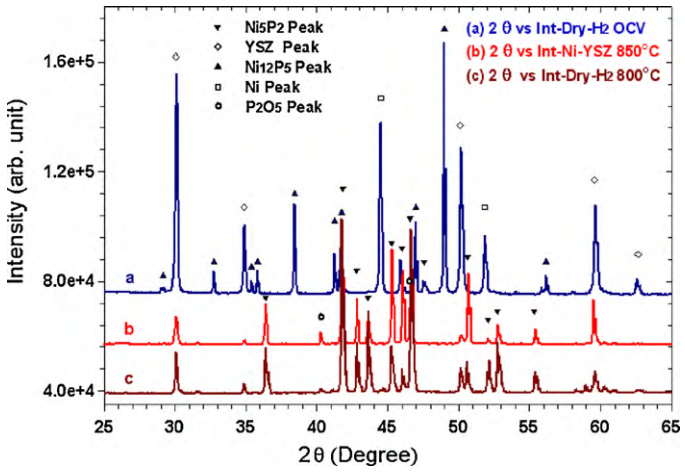

Fig. 15. The XRD spectra of the top cell anode surface after exposure to 10 ppm PH_3 in (a) dry H_2 at 800 °C without load compared to (b) syngas fuel at 850 °C using the Ni-YSZ disc and (c) dry H_2 at 800 °C with load.

Table 3
P_{2p} and Ni $_{2p3/2}$ peak positions in different regions of the Ni-YSZ anodes tested in syngas and dry H_2 (cell-2) at different temperatures.

Type of binding	Measured BE (eV)[a]	Region	Reference BE (eV)	Reference
P in PO_4^{3-}	133.4–133.7	Cross-section	132.9–134.7	[10]
P in elemental phosphorus	130.0–130.2	Surface	129.9–130.4	[10,11]
P in nickel phosphide	129.7–129.8	Surface	129.1–129.5	[11,12]
Ni metallic	852.7–853.0	Surface	852.0–852.9	[10,11]
NiO	–	–	853.4–854.4	[10]
$Ni(OH)_2$	855.5–856.3	Interface	855.6–855.9	[12]

[a] The peak position was calibrated according to the standard C1s position (284.8 eV).

near the anode/electrolyte interface, in the middle of the anode cross-section, near the anode surface and at the surface of the shiny layer. The assignment of elemental valence states according to binding energy (BE) is summarized in Table 3 by comparison with referenced reports. The detailed XPS scans of the 2p spectra for phosphorus at the surface and cross-section of the PH_3-poisoned Ni-YSZ anodes are shown in Figs. 16 and 17 to investigate the nature of the bonding between Ni and P and the impact of testing conditions on the anode phase transitions. Shown in Fig. 16 are the XPS spectra of the P_{2p} region for different locations on the cross-section of Ni-YSZ anodes. It can be seen that all the spectra taken near the anode/electrolyte interface display only one phosphorus peak at BE around 133.3–133.7 eV, corresponding to phosphorus in the phosphate state [10]. This indicates that despite different testing conditions, P tends to be in an oxidized state near the anode/electrolyte interface. As the spectra were taken across the Ni-YSZ anode from the middle towards the near-surface region, a second P peak with lower BE around 130.1–129.7 eV becomes more evident. The peak position matches well with elemental phosphorus and phosphide (unoxidized phosphorus)[10–13]. Although the phosphate-like P peak was found dominant over the phosphide-like P peak in the cross-section for all the tested samples, only the spectra of the cell-2 tested in dry H_2 displayed a new dominant P peak at lower BE of 132.5 eV and a shift of the phosphide-like peak towards lower values. By comparison with the P_{2p} spectra taken on the anode surface as in Figs. 16 and 17, the intensity of the phosphide-like P peaks became much stronger, and the BE position

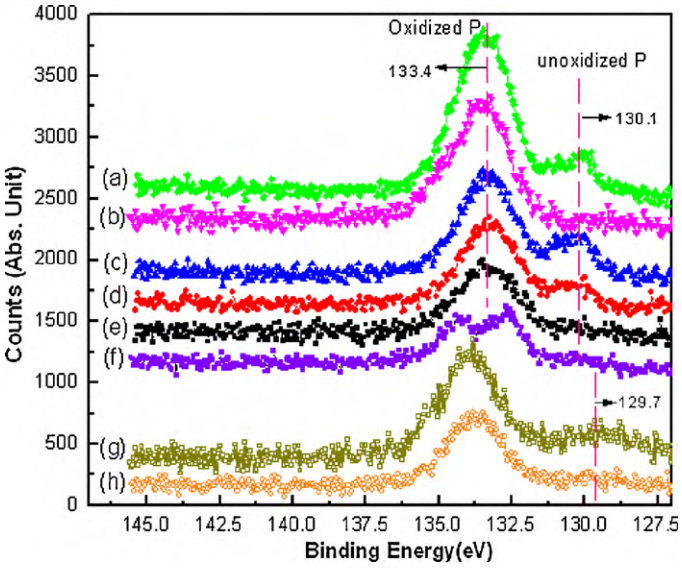

Fig. 16. XPS spectra of phosphorus for different cross-sectional regions of the Ni-YSZ anodes tested at various conditions. (a) 750 °C syngas, near the anode surface; (b) 750 °C syngas, near the anode/electrolyte interface; (c) 850 °C syngas, near the anode surface; (d) 850 °C syngas, in the middle of the anode; (e) 850 °C syngas, near the anode/electrolyte interface; (f) dry H_2 at 800 °C, near anode surface; (g) dry H_2 at 800 °C, in the middle of the anode; (h) dry H_2 at 800 °C, near the anode/electrolyte interface.

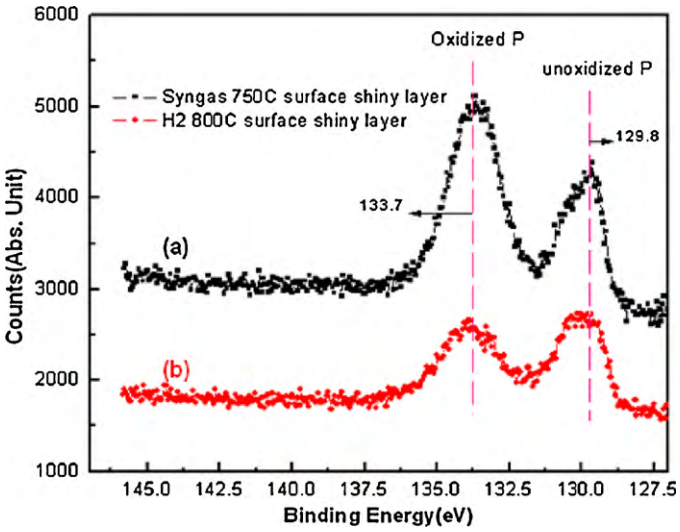

Fig. 17. XPS spectra of phosphorus for the "shiny" nickel phosphide layers deposited at the surface of the Ni-YSZ anodes tested in (a) syngas at 750 °C and in (b) dry hydrogen at 800 °C.

was also 0.2–0.3 eV more negative than that of the cross-section peak. Thus the lower valence state of surface phosphorus seems to fall between the values of unoxidized phosphorus. The discrepancy on P states from XPS results and XRD results will be discussed in Section 4.

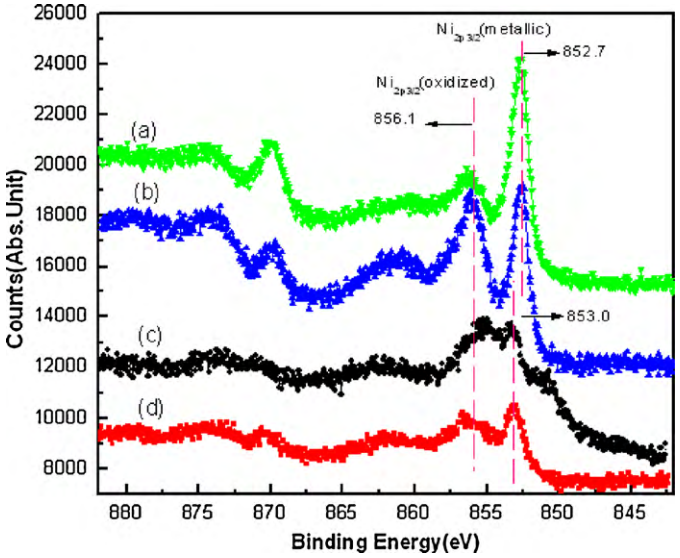

Fig. 18. XPS spectra of Ni in the cross-section and at the surface of the Ni-YSZ anodes tested in syngas at 750 °C and in dry H_2 at OCV at 800 °C (a) H_2 800 °C, surface "shiny" layer; (b) syngas 750 °C, surface shiny layer; (c) syngas 750 °C, cross-section near anode/electrolyte interface; (d) syngas 750 °C, cross-section near anode surface.

On the other hand, Fig. 18 shows the $Ni_{2p3/2}$ spectra split into two BE peaks at 852.7–853.2 eV (corresponding to metallic Ni) and 855.6–856.0 eV (corresponding to oxidized Ni) both at the anode surface and cross-section. So it is obvious that the Ni exists as a mixture of metallic Ni and oxidized Ni across the entire anode layer [10,11]. The oxidized Ni could be in multiple oxide forms, hydroxide and phosphate, for example [12]. The metallic Ni peak at the surface was observed to shift 0.4–0.5 eV negatively from that in the cross-section, and become dominant over the oxidized Ni peak at the surface for the cell tested in dry H_2.

4. Discussion

The main phosphorus phases for the PH_3-poisoned anodes were identified as Ni_5P_2 and $Ni_{12}P_5$ by XRD analysis, while the above XPS results indicated the dominant forms of phosphorus were phosphate in the anode cross-section and a mixture of both unoxidized phosphorus and phosphate at the anode surface. However, such discrepancy on the P states may mainly reflect the different detection limits of the two techniques, rather than contradicting the major finding of Ni_xP_y as the product of PH_3 poisoning in this and other studies. As XPS is a much more surface sensitive technique with significantly less penetration depth (<10 nm) compared to that of XRD (10–50 μm), the XRD results should be more representative of the bulk phase analysis for the entire anode layer. Moreover, our previous thermodynamic calculation predicted Ni_xP_y as the predominant phase for anode degradation under these testing conditions. On the other hand, the XRD analysis gives no details about the distribution of the phosphorus states at specific regions of interest along the anode. In this case comparison of XPS spectra at the anode surface and cross-section will be useful to understand the interaction of Ni and P during anode degradation.

The XPS study showed formation of phosphate species on both the anode surface and cross-section, which can result from the reaction of nickel phosphide to phosphate upon exposure to ambient air at room temperature:

$$Ni_5P_2(s) + 4O_2(g) + 2H_2O(l) = Ni_3(PO_4)_2(s) + 2Ni(OH)_2(s), \quad \Delta G_{300\,K} = -4104.6\,kJ\,mol^{-1} \tag{1}$$

$$0.4Ni_{12}P_5(s) + 4.9O_2(g) + 1.8H_2O(l) = Ni_3(PO_4)_2(s) + 1.8Ni(OH)_2(s), \quad \Delta G_{300\,K} = -2089.48\,kJ\,mol^{-1} \tag{2}$$

Such oxidation of surface P to form phosphate compounds was commonly found in research on nickel phosphides. The reaction for the surface oxidation is reported to occur in as fast as several minutes in air at room temperature [14]. The XRD spectra also show the weak P_2O_5 peak. Thus the presence of surface phosphate seems almost inevitable for the non-destructive XPS measurement, and it cannot be determined here whether there was phosphate formed in situ during the anode degradation or during the post-mortem exposure to ambient air. However the fact that unoxidized phosphorus peaks tend to be rich at the cell anode surface while absent at anode/electrolyte the interface may partially reveal the influence of the local electrochemical reaction and consequent oxygen ion distribution from the interface to the surface on the Ni-YSZ anode. The presence of unoxidized phosphorus indicates nickel phosphides are rich at the surface and near-surface regions; hence some "residual" phosphide-like species may still exist after surface oxidation in air at room temperature. At the active electrochemical reaction zone through which an excessive oxygen ion flux passes, less phosphide compounds were expected and consequently only phosphorus in higher oxidation states can be seen. Reactions (1) and (2) could be very favorable during the cell cool-down period after the PH_3 flow was cut off and the oxygen ion concentration was still significant at the anode/electrolyte interface. In this way the XPS analysis showed that the interaction of Ni with P might be sensitive to the intrinsic electrochemical reactions of the anode interface. It can be also noted that the lower valence state of phosphorus for the dry H_2 cell-2 anode was closer to that of phosphide than the syngas-tested anodes, and the amount of surface unoxidized phosphorus also increased relatively. So a greater tendency for the formation of nickel phosphide can be expected for the anode without the presence of H_2O.

From thermodynamic calculations, the reaction between PH_3 and Ni is more favorable at 750 °C than at 850 °C because the changes of Gibbs free energy (ΔG) are more negative in these reactions ($\Delta G_{750\,°C} = -293.4\,kJ\,mol^{-1}$ and $\Delta G_{850\,°C} = -280.3\,kJ\,mol^{-1}$, these values are calculated for 10 ppm PH_3 in syngas). The SEM images in Fig. 4 also showed that the formation of Ni_xP_y on the cell surface is more abundant for the syngas at 750 °C case which produced a 55 μm thick shiny layer detached from the cell anode base. From the cell electrochemical performance data in Fig. 1, the cell degradation rate is higher for the 850 °C case. Thus the PH_3 poisoning is more damaging at the higher cell working temperature. The cell initial performance and the cell electrochemical reaction rates of these two cases are similar under a load of 0.5 A cm^{-2} with the same syngas fuel except for the temperature difference. If more PH_3 was consumed at the anode surface for 750 °C, then less PH_3 could reach the interface to destroy the triple phase boundary. On the other hand, the diffusion coefficient for PH_3 into Ni and the anode interface is temperature dependent ($\exp(-1/kT)$). Thus a higher temperature gives the PH_3 molecules a higher diffusion coefficient. The larger increase of the cell total cell resistance ΔR_{total} at 850 °C results from PH_3 penetrating to the cell anode/electrolyte interface faster at 850 °C than at 750 °C. Compared with the increase of total cell resistance after the cell is exposed to PH_3, the increase of the cell ohmic resistance is very small (see Table 1). The surface reconstruction of the anode over about 200 h did not significantly degrade the anode electronic conductivity. The production of Ni_xP_y on the cell surface may not affect the cell performance as quickly as it does for attack at the anode interface leading to reduced TPB length. So it is hypothesized that the higher degradation rate for the 850 °C case than that for the 750 °C case during 200 h of PH_3 poisoning is due mainly to reaction at the TPB. However, the anode reconstruction and nickel migration will mainly contribute to the cell degradation by reducing the anode porosity and conductivity with increasing exposure time to PH_3.

The dry H_2 cell-2 without load provided additional evidence that a dense shiny Ni_xP_y layer over 50 μm thick was formed and subsequently detached from the base anode. Comparing with the dry H_2 cell-1 with load, the cell-2 test had a rich Ni_xP_y production on the anode surface. The intensive electrochemical reaction on cell-1 provided sufficient H_2O vapor on the anode surface which could cause partial PH_3 oxidation and suppress the production of Ni_xP_y. Since there was no intensive electrochemical reaction on the cell-2 anode, more Ni_xP_y formed on the anode surface. Similarly, the case of the Ni-YSZ cermet disc exposed to humidified syngas with PH_3 for 120 h at 850 °C showed a thick Ni_xP_y layer built up as a shiny bubble, 86 μm thick, on the Ni-YSZ surface (Fig. 7). Because there were no electrochemical reactions or oxygen ion concentration on the disc, the Ni_xP_y production on the Ni-YSZ disc is much more pronounced than for that of the syngas 850 °C case when current was being drawn. Moreover, the back side of the Ni-YSZ disc in Fig. 7(b) did not show any Ni_xP_y which implies that the reaction between Ni and PH_3 occurs intensively on the surface rather than throughout the inner part of the disc.

5. Conclusion

The long-term test of a Ni-YSZ anode-supported SOFC cell exposed to syngas and dry H_2 with 10 ppm PH_3 impurity has been evaluated under different cell working conditions. The 10 ppm PH_3 in syngas and H_2 fuel is favored to react with the nickel in the Ni-YSZ anode to produce nickel phosphides whether or not H_2O or electrochemical reactions are present. 10 ppm PH_3 in syngas is more reactive with Ni in the anode at lower working temperature and produces a rich secondary Ni_xP_y phase. However, the cell degradation rate is larger at the higher cell working temperature during the initial 200 h test suggesting more attack at TPB as a result of enhanced diffusion of PH_3. The water vapor generated by intense electrochemical reaction can partially suppress Ni_xP_y products on the cell anode surface. The dominant compositions of Ni_xP_y on the cell anode are Ni_5P_2 with the presence of H_2O, and $Ni_{12}P_5$ without the presence of H_2O. Phosphate phases can appear on the PH_3-poisoned post-mortem cell anode after being exposed to air or by reaction with the oxygen ions near the anode/electrolyte interface.

Acknowledgements

This work is conducted under US DOE (Department of Energy) EPSCoR Program. It is jointly sponsored by US DOE Office of Basic Energy Sciences, NETL (National Energy Technology Laboratory), WV State EPSCoR Office and the West Virginia University under grant number DE-FG02-06ER46299. Dr. Tim Fitzsimmons is the DOE Technical Monitor. Dr. R. Bajura is the Administrative Manager and Dr. I. Celik is the Technical Manager and Principal Investigator of this project. Mr. Liviu Magean and Mrs. Andrienne MacLeod are thanked for taking the SEM, EDS and XRD data.

References

[1] C. Xu, J. Zondlo, H. Finklea, O. Demircan, M. Gong, X. Liu, Journal of Power Sources 193 (2009) 739–746.
[2] O. Demircan, W. Zhang, C. Xu, J. Zondlo, H. Finklea, Journal of Power Sources 195 (2010) 3091–3096.
[3] J.P. Trembly, Ph.D. Dissertation, Investigation into the effects of trace coal syngas species on the performance of solid oxide fuel cell anodes, The Russ College of Engineering and Technology of Ohio University, 2007.
[4] L.R. Pederson, O.A. Marina, X. Zhou, Y. Chou, G.W. Coffey. V.9 SECA Coal-Based Systems Core Research. V. Advanced Research, DOE FY 2007 Annual Report.
[5] G.S. Saini, L.D. Calvert, J.B. Taylor, Canadian Journal of Chemistry 42 (7) (1964) 1511–1517.
[6] M. Yousuf, P.C. Sahu, H.K. Jajoo, S. Rajagopalan, K.G. Rajan, Journal of Physics, F 16F (1986) 373–378.
[7] J.D. Hanawalt, H.W. Rinn, L.K. Frevel, Industrial & Engineering Chemistry. Analytical Edition 10 (9) (1938) 457–512.
[8] M. Yashima, S. Sasaki, M. Kakihana, Acta Crystallographica Section B 50 (1994) 663–672.
[9] S. Rundqvist, E. Larsson, Acta Chemica Scandinavica 13 (1959) 551.
[10] J.F. Moulder, W.F. Stickle, P.E. Sobol, K.D. Bomben, Handbook of X-ray Photoelectron Spectroscopy, Physical Electronics, Eden Prairie, MN, 1995.
[11] V.I. Nefedov, Y.V. Salyn, E.P. Domashevskaya, Y.A. Ugai, V.A.J. Terekhov, Electron Spectroscopy and Related Phenomena 6 (1975) 231.
[12] M.G. Thube, S.K. Kulkarni, D. Huerta, A.S. Nigavekar, Physical Review B 34 (10) (1986) 6874–6878.
[13] J. Okado, M. Shima, I.R. McColl, R.B. Waterhouse, T. Hasegawa, M. Kasaya, Wear 225–229 (1999) 749–757.
[14] Z. Qi, W. Lee, Tribology International 43 (2010) 810–814.